nature catalysis

Article

https://doi.org/10.1038/s41929-023-00990-9

Activation of light alkanes at room temperature and ambient pressure

In the format provided by the authors and unedited

Table of Content

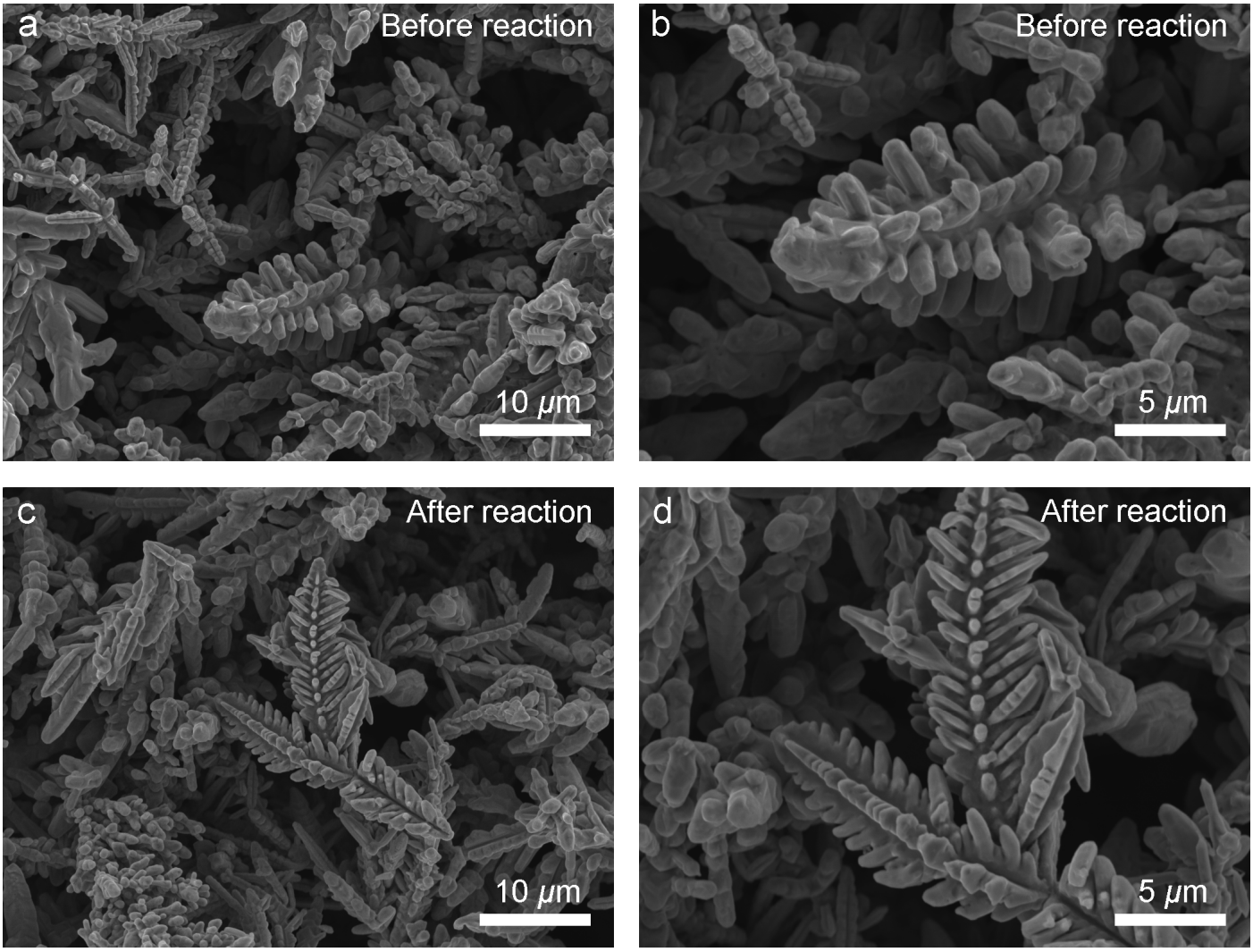

Supplementary Fig. 1 | SEM images of pristine Cu powder (**a**, **b**) and Cu powder after ethane activation for 1 hour at 0.2 O_2 mole fraction with 20 $mg \cdot mL^{-1}$ Cu loading in 1.0 M $HClO_4$ (**c**, **d**).

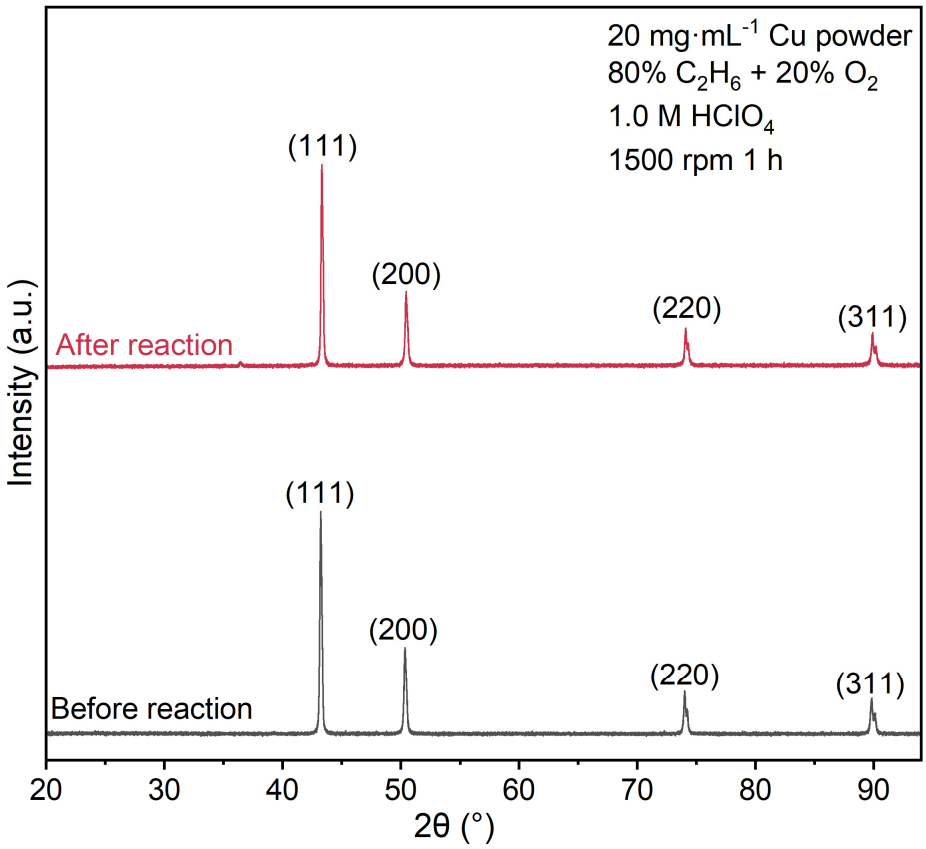

Supplementary Fig. 2 | XRD patterns of pristine Cu powder and Cu powder after ethane activation for 1 hour at 0.2 O_2 mole fraction with 20 $mg \cdot mL^{-1}$ Cu loading in 1.0 M $HClO_4$.

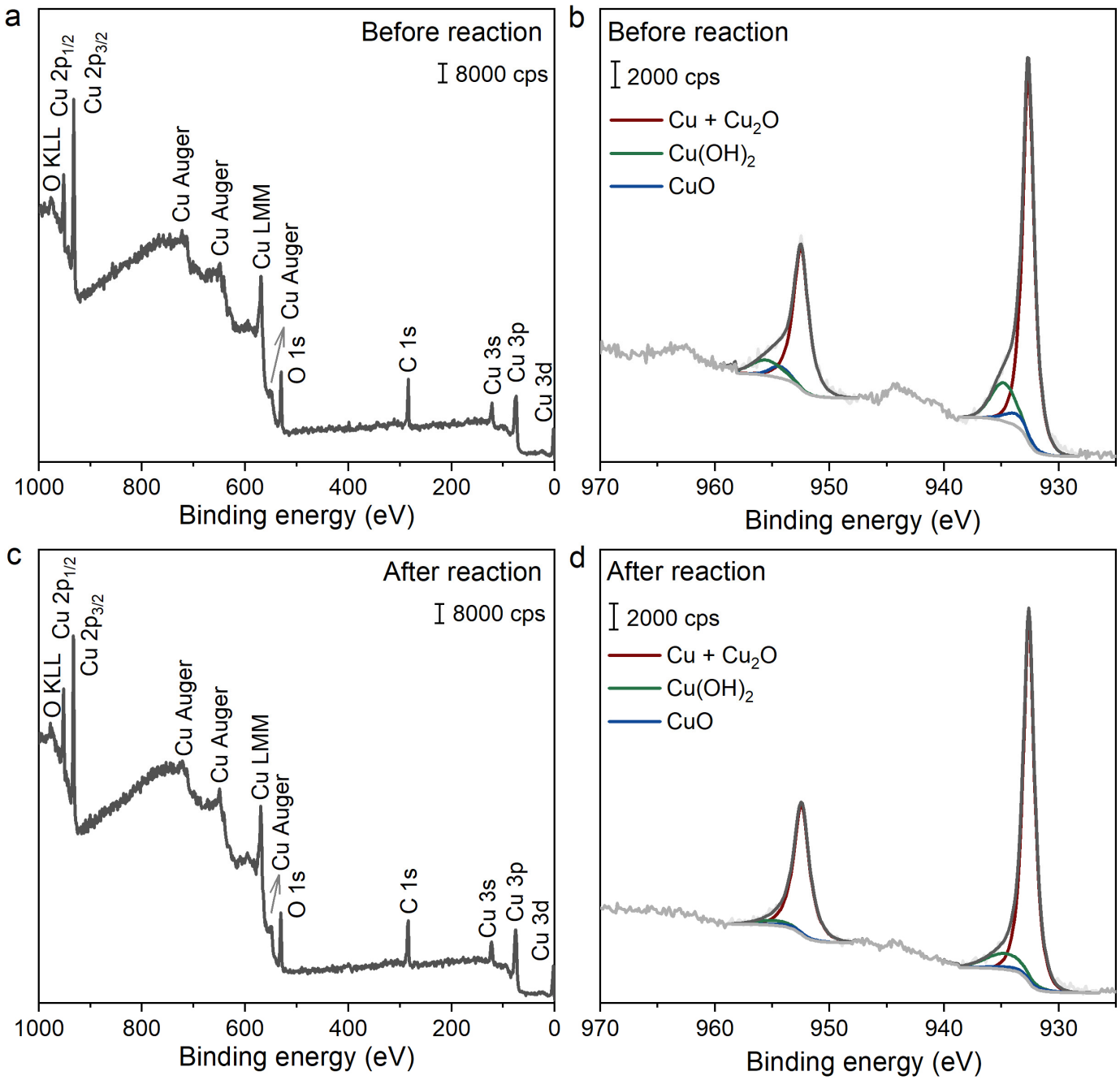

Supplementary Fig. 3 | XPS spectra of pristine Cu powder (**a**, **b**) and Cu powder after ethane activation for 1 hour at 0.2 O_2 mole fraction with 20 mg·mL^{-1} Cu loading in 1.0 M $HClO_4$ (**c**, **d**).

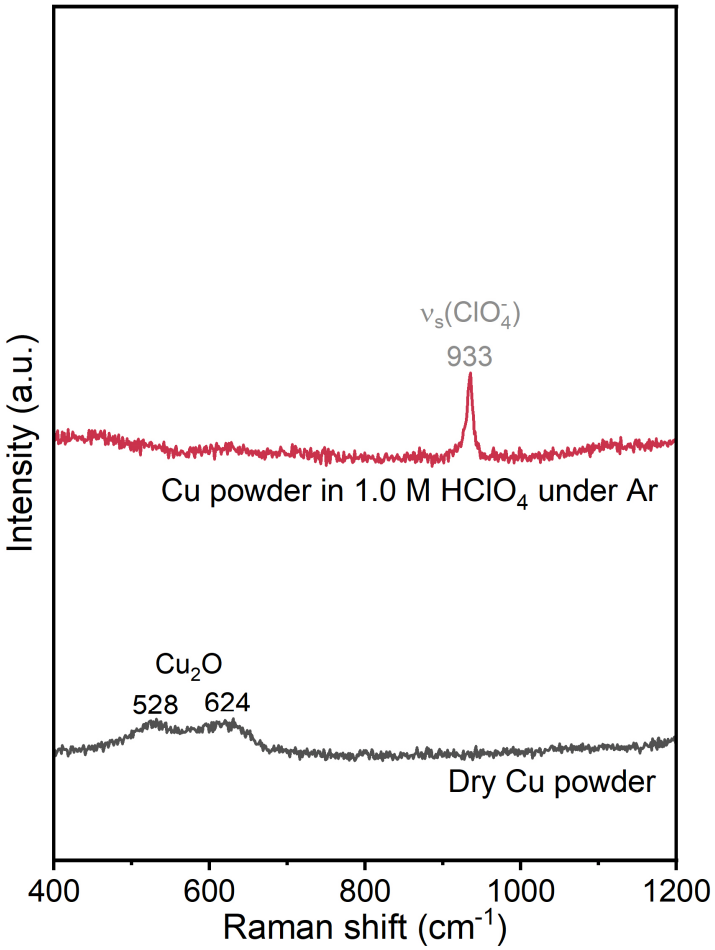

Supplementary Fig. 4 | Raman spectra of pristine Cu powder and Cu powder in 1.0 M $HClO_4$.

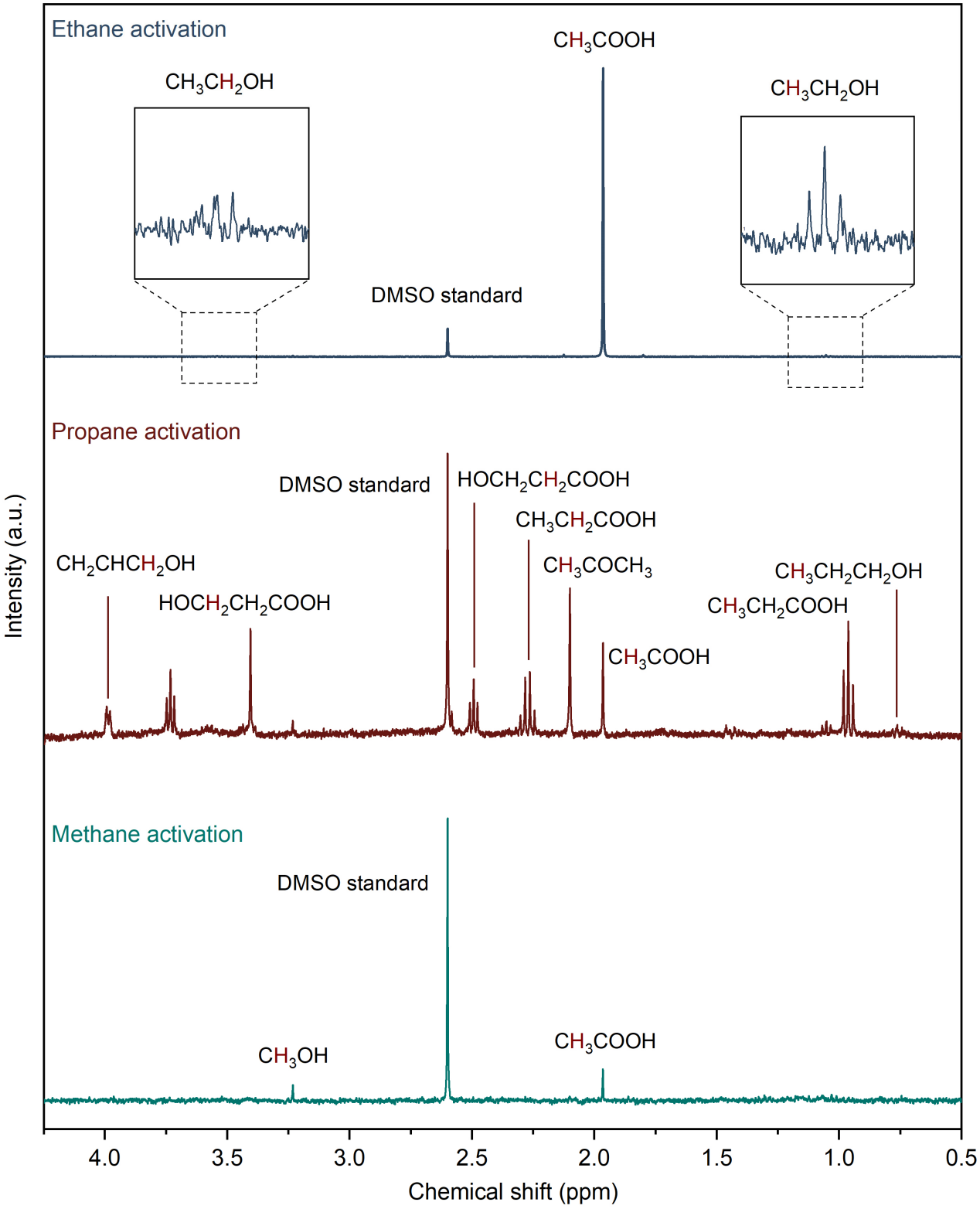

Supplementary Fig. 5 | NMR spectra of ethane, propane and methane activation for 1 hour at 0.2 O_2 mole fraction with 20 mg·mL^{-1} Cu powder in 1.0 M $HClO_4$. The concentration of DMSO standard in all samples was 50 μM.

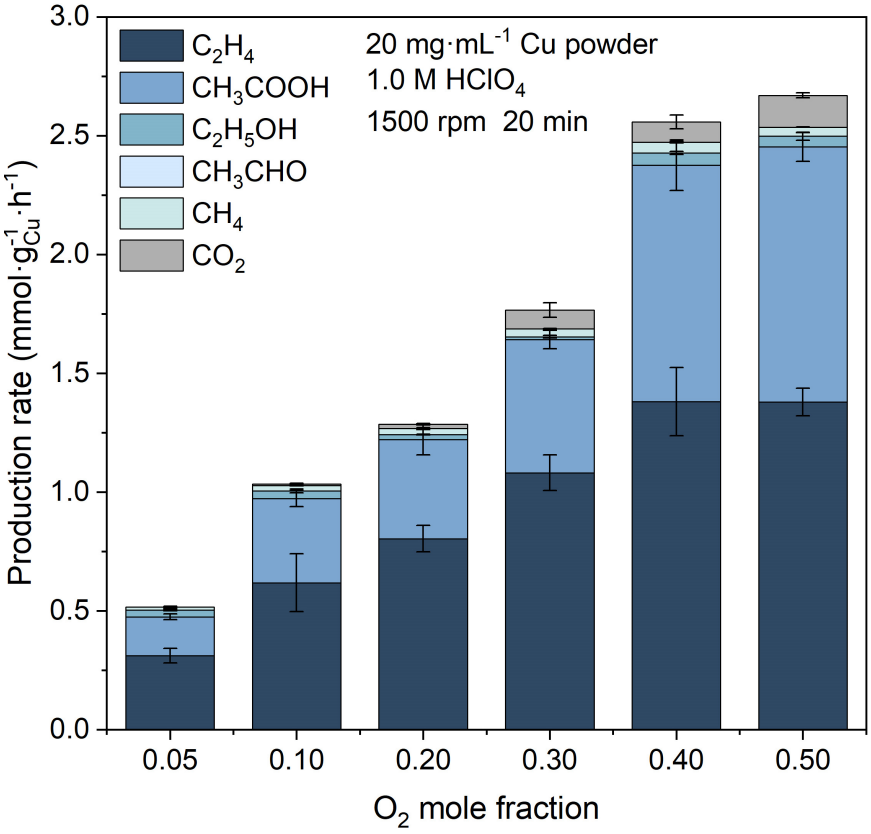

Supplementary Fig. 6 | The production rate and distribution of ethane activation with different mole fractions of O_2 in gas feed. Error bars represent the standard deviation of four independent measurements, and the data are presented as mean values ± standard deviation.

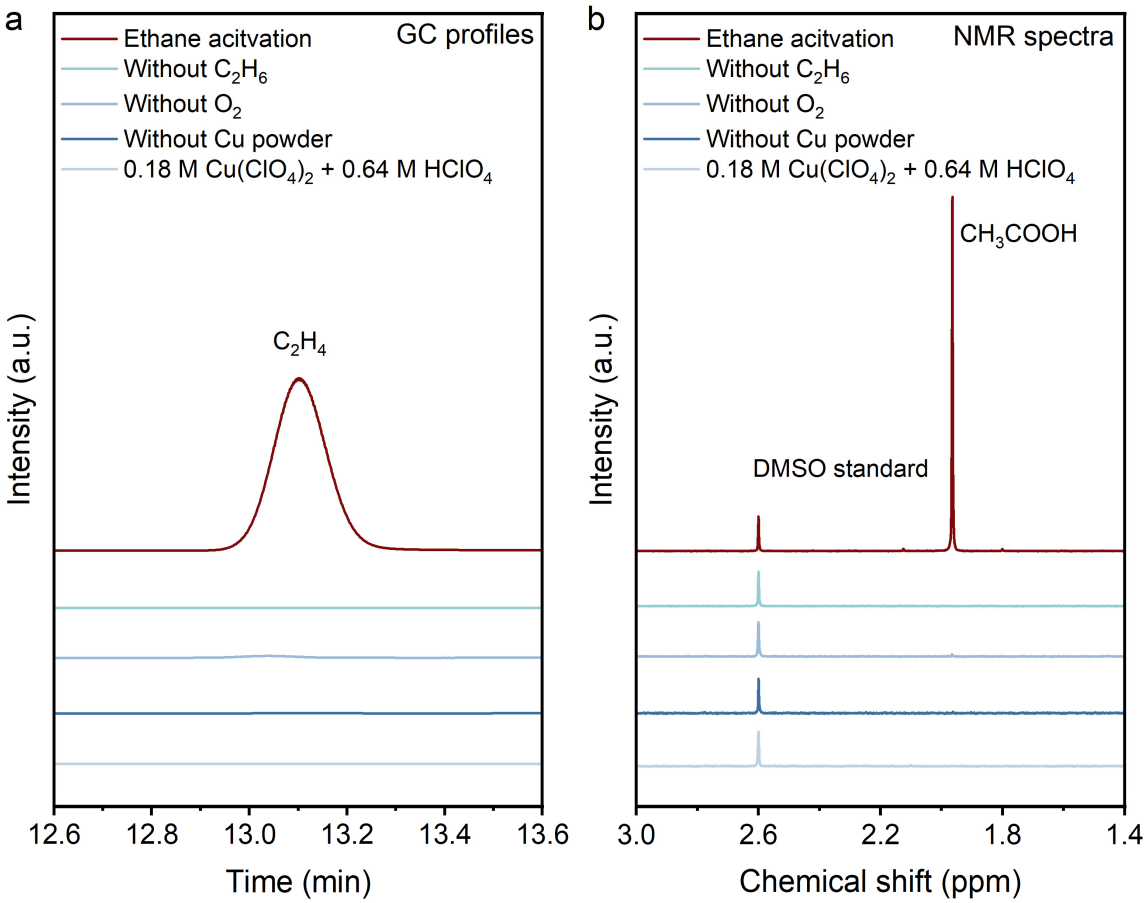

Supplementary Fig. 7 | GC profiles (**a**) and NMR spectra (**b**) for control experiments of ethane activation with ethane, O_2 or Cu powder was absent in the reaction system. The ethane activation data was obtained at 20 mg·mL^{-1} Cu powder in 1.0 M $HClO_4$ with ethane and O_2 mole ratio of 8:2. The trace amounts of products in experiments without O_2 are likely due to a slight ambient air filtration to the system during reaction. In experiments using Cu^{2+} ions instead of Cu powder, the concentration of Cu^{2+} of 0.18 M was chosen to match the final concentration of Cu^{2+} after ethane activation (**Supplementary Table 10**). See Methods for more experimental details.

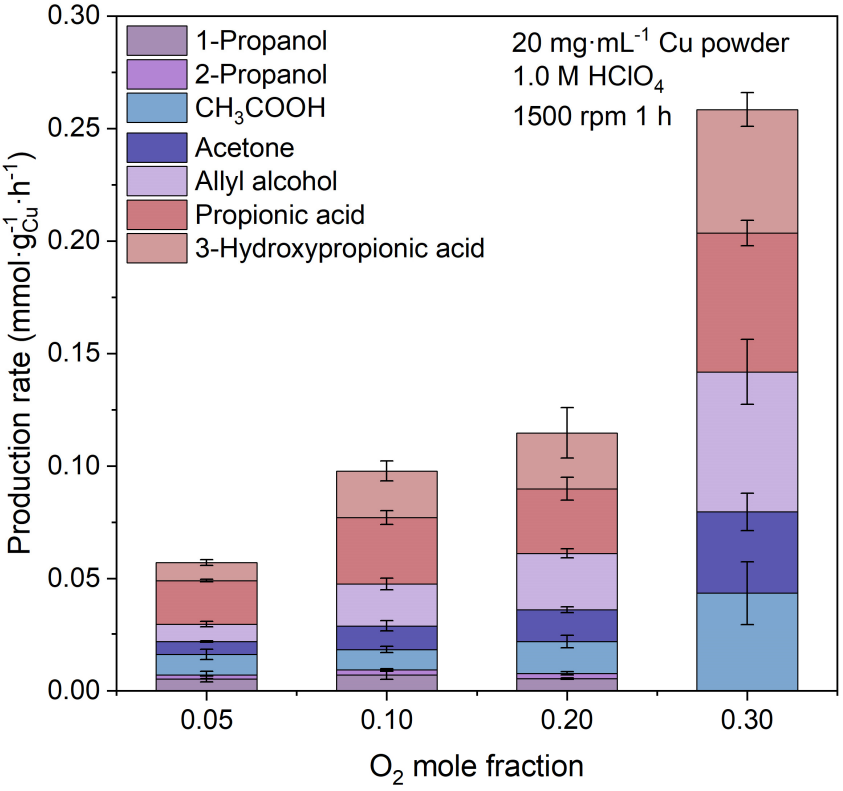

Supplementary Fig. 8 | The production rate and distributions of minor products in propane activation at different O_2 mole fractions in 1.0 M $HClO_4$ with 20 mg·mL^{-1} Cu powder. Error bars represent the standard deviation of four independent measurements, and the data are presented as mean values ± standard deviation.

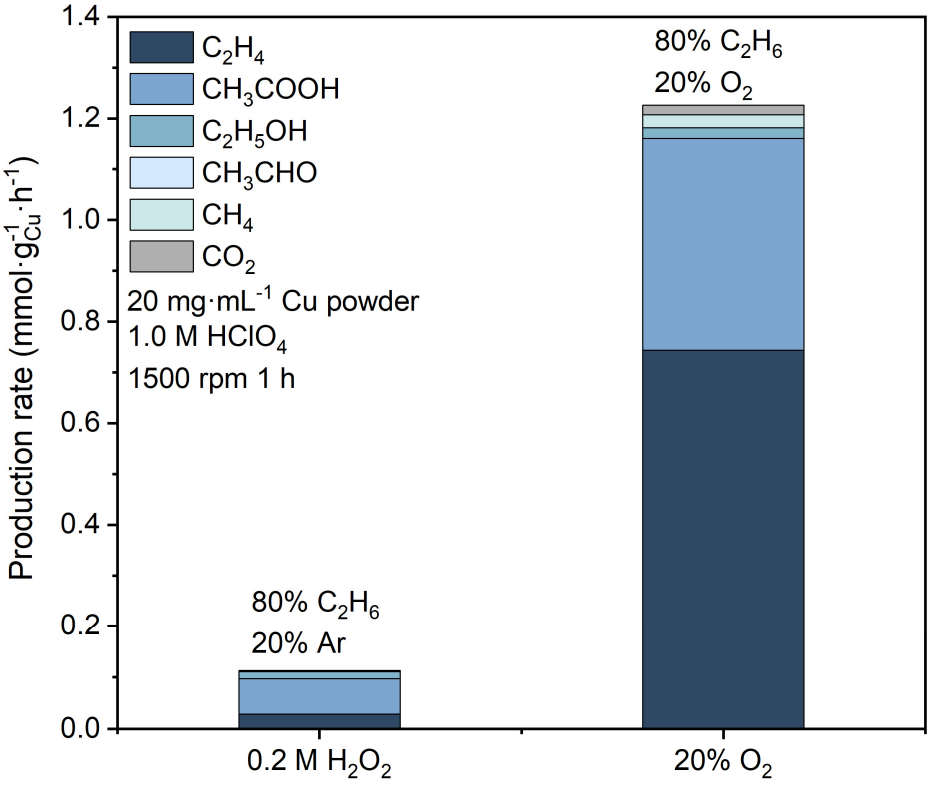

Supplementary Fig. 9 | Comparisons of ethane activation performance using H_2O_2 or O_2 as the oxidant.

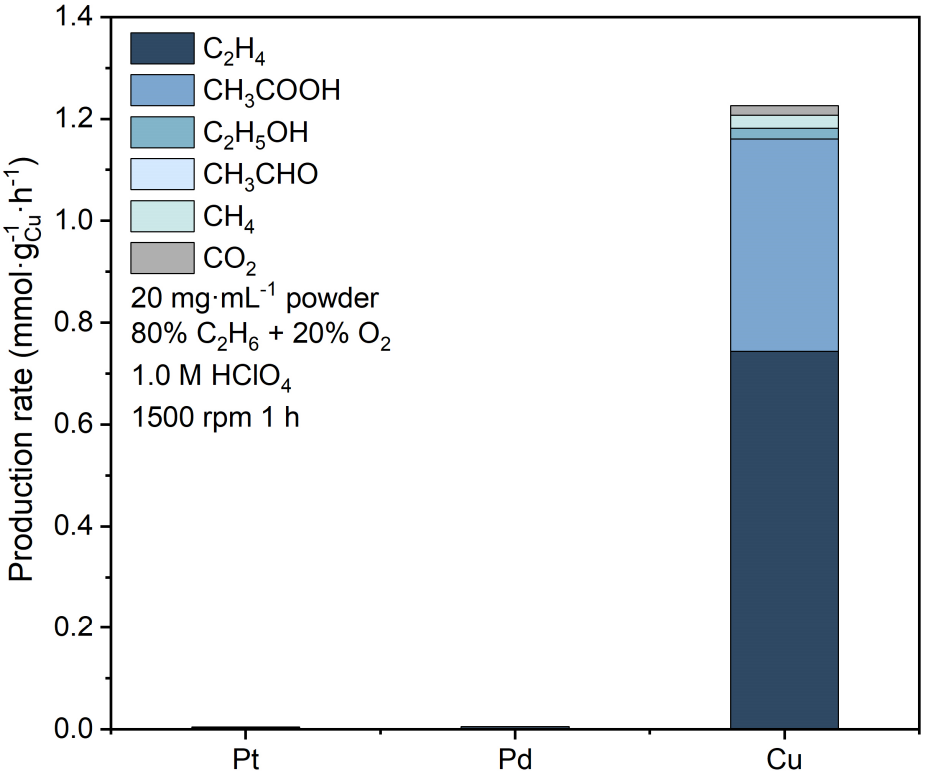

Supplementary Fig. 10 | Comparisons of ethane activation performance in 1.0 M $HClO_4$ at 0.2 O_2 mole fraction using 20 mg·mL^{-1} Cu, Pt, and Pd powder as the catalyst.

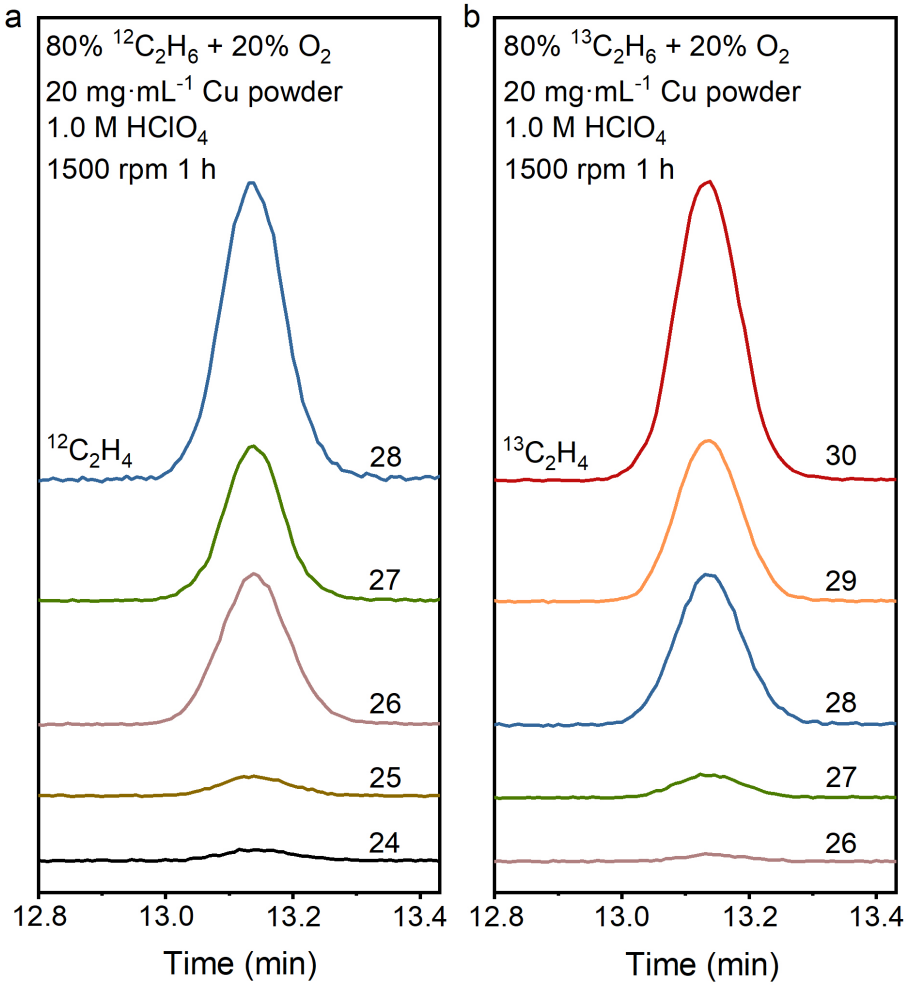

Supplementary Fig. 11 | Mass spectrometry profiles of produced C_2H_4 using $^{12}C_2H_6$ (**a**) or $^{13}C_2H_6$ (**b**) as gas feed.

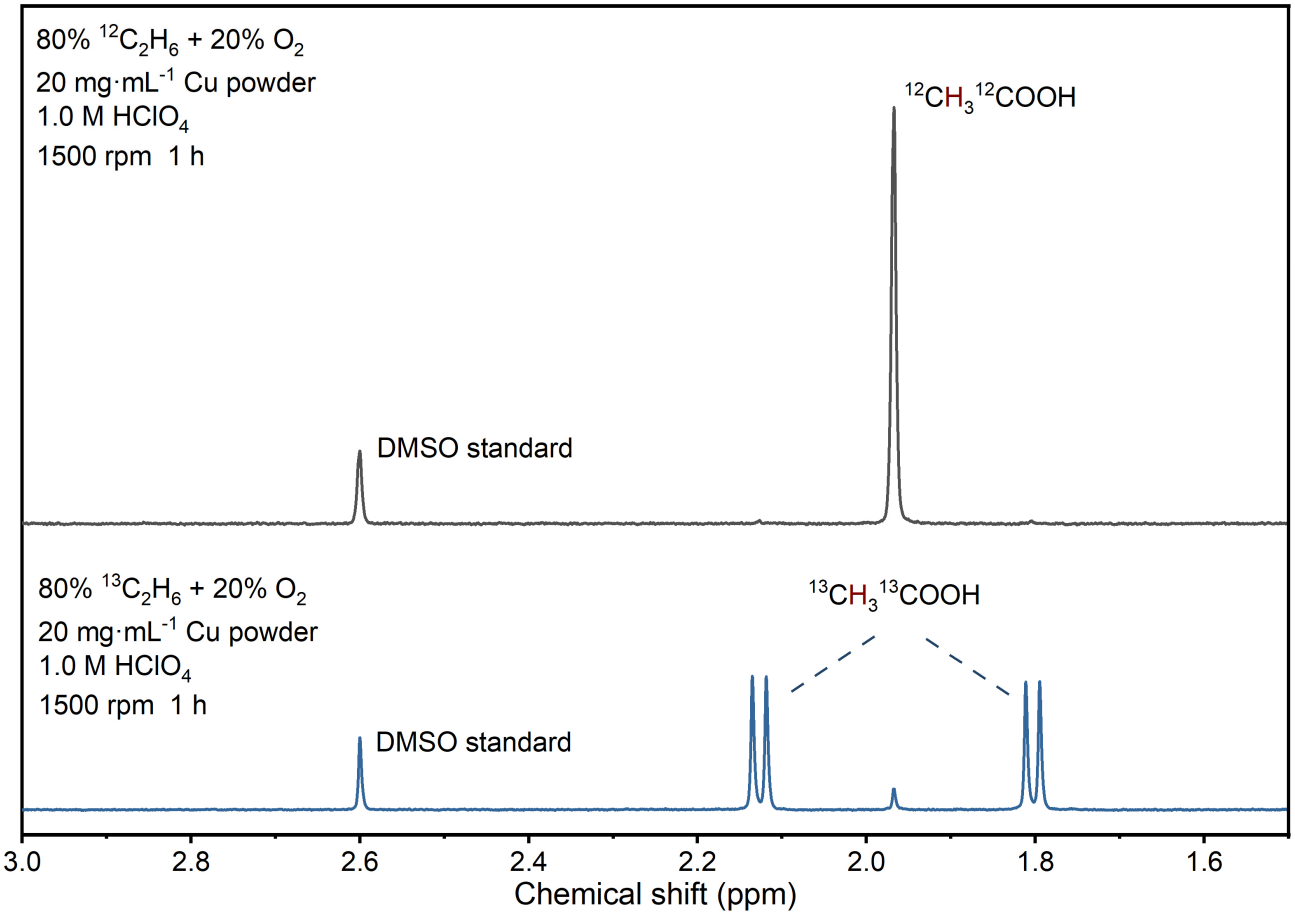

Supplementary Fig. 12 | NMR spectra of produced acetic acid using $^{12}C_2H_6$ or $^{13}C_2H_6$ as gas feed.

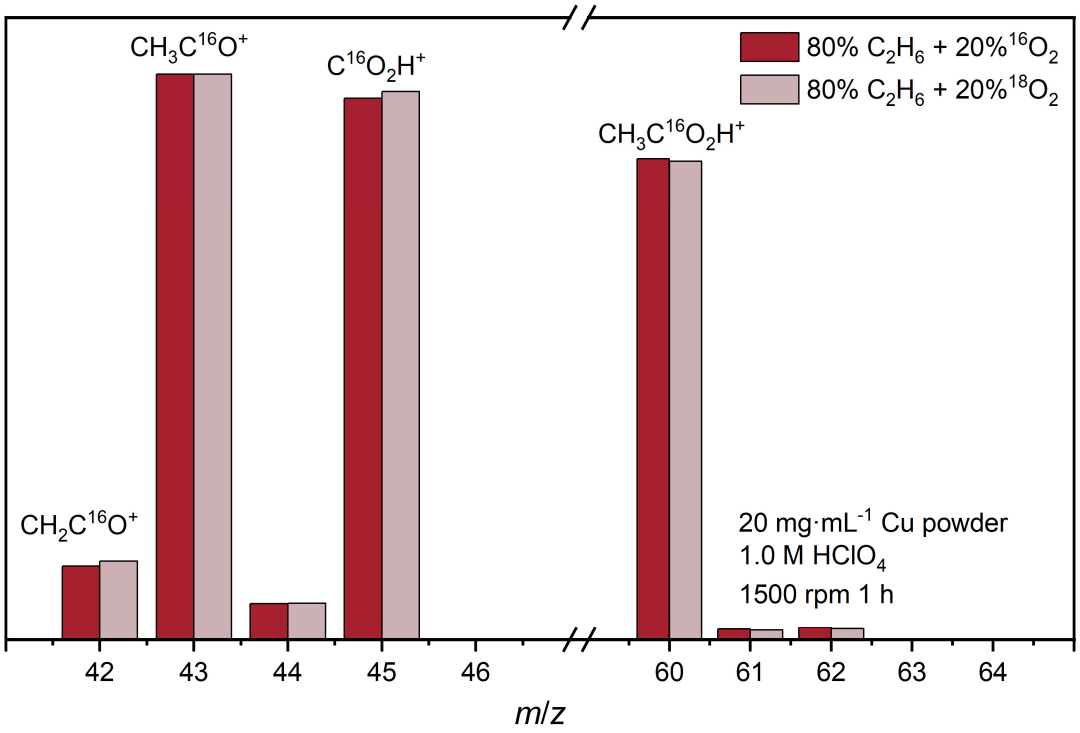

Supplementary Fig. 13 | Mass spectrometry profiles of produced acetic acid using $^{16}O_2$ or $^{18}O_2$ as gas feed.

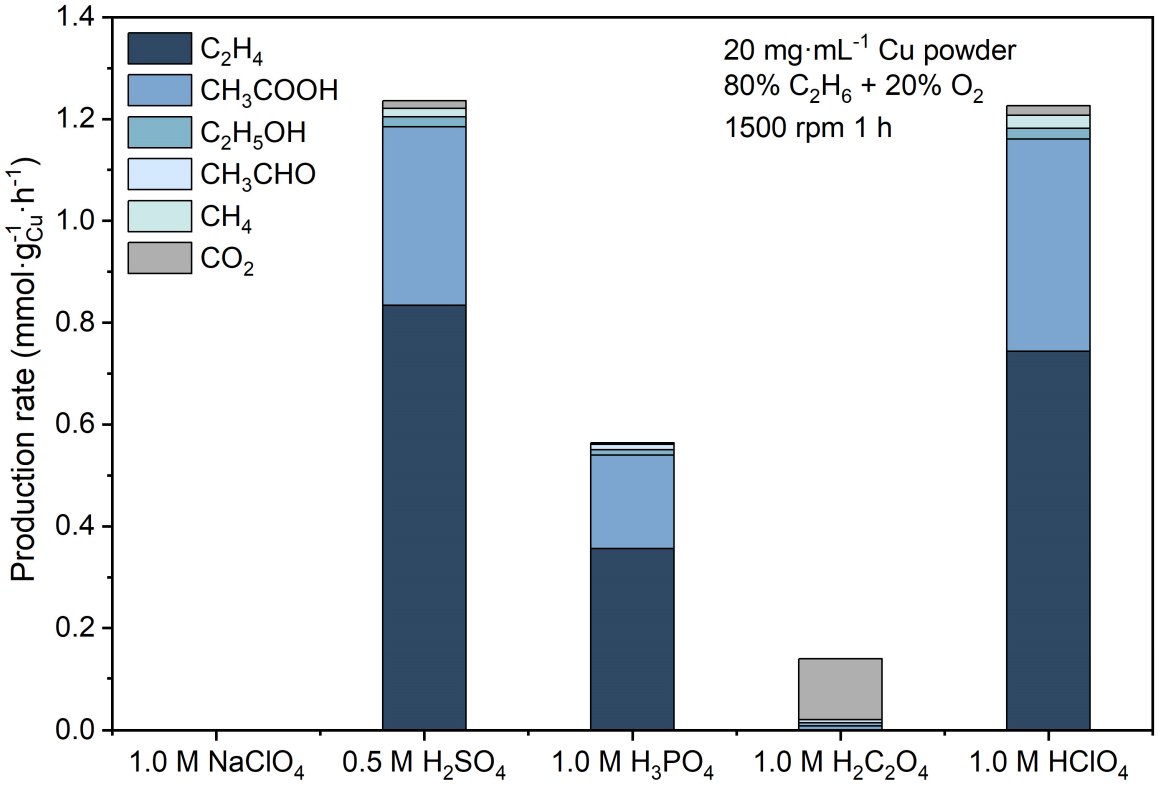

Supplementary Fig. 14 | Comparisons of production rates between ethane activation conducted in 1.0 M $HClO_4$, 0.5 M H_2SO_4, 1.0 M $NaClO_4$, 1.0 M H_3PO_4 or 1.0 M $H_2C_2O_4$ at 0.2 O_2 mole fraction with 20 mg·mL^{-1} Cu powder.

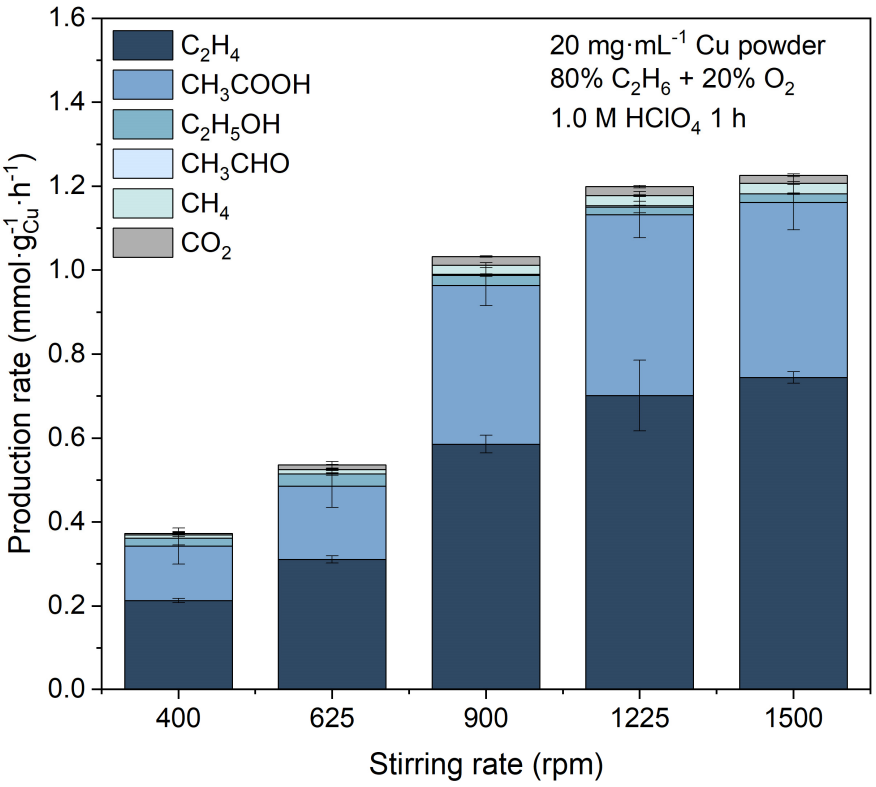

Supplementary Fig. 15 | The product rate and distribution of ethane activation with different stirring rates in 1.0 M $HClO_4$ at 0.2 O_2 mole fraction with 20 mg·mL^{-1} Cu powder. Error bars represent the standard deviation of four independent measurements, and the data are presented as mean values ± standard deviation.

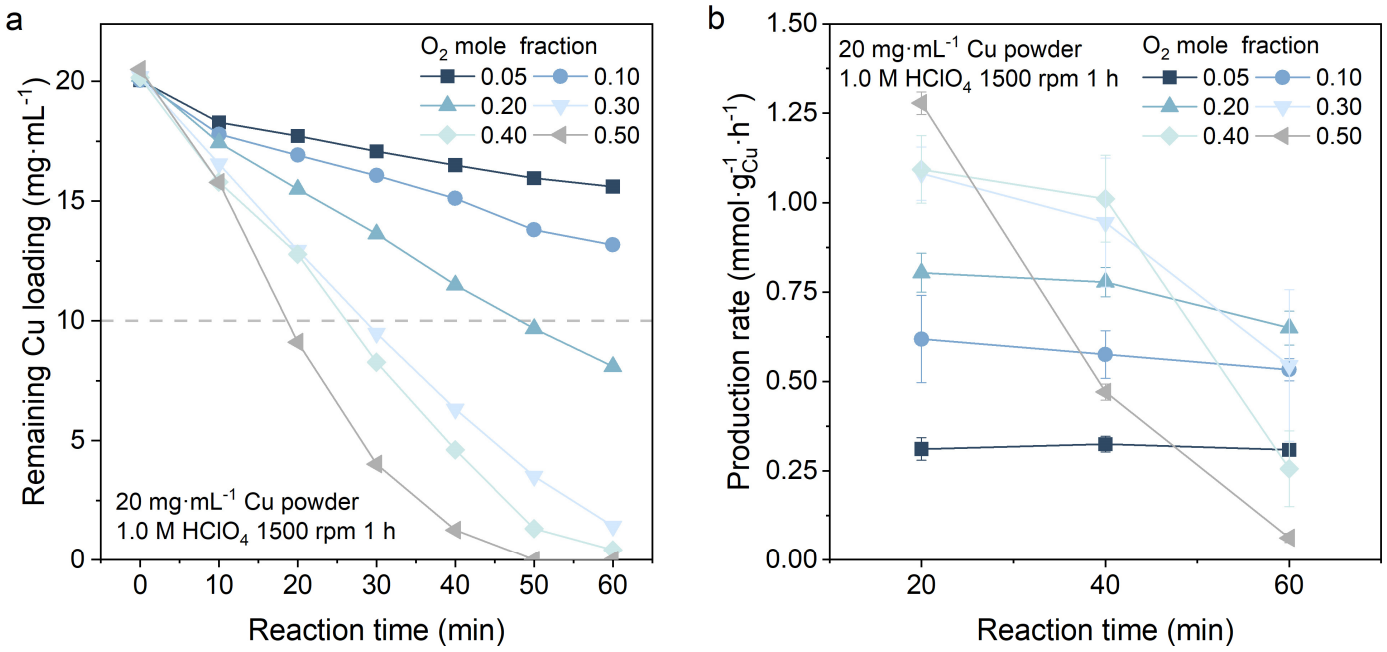

Supplementary Fig. 16 | a, Remaining Cu loading and **b,** ethylene production rates as a function of reaction time and oxygen mole fraction in gas feed. Error bars represent the standard deviation of four independent measurements, and the data are presented as mean values ± standard deviation.

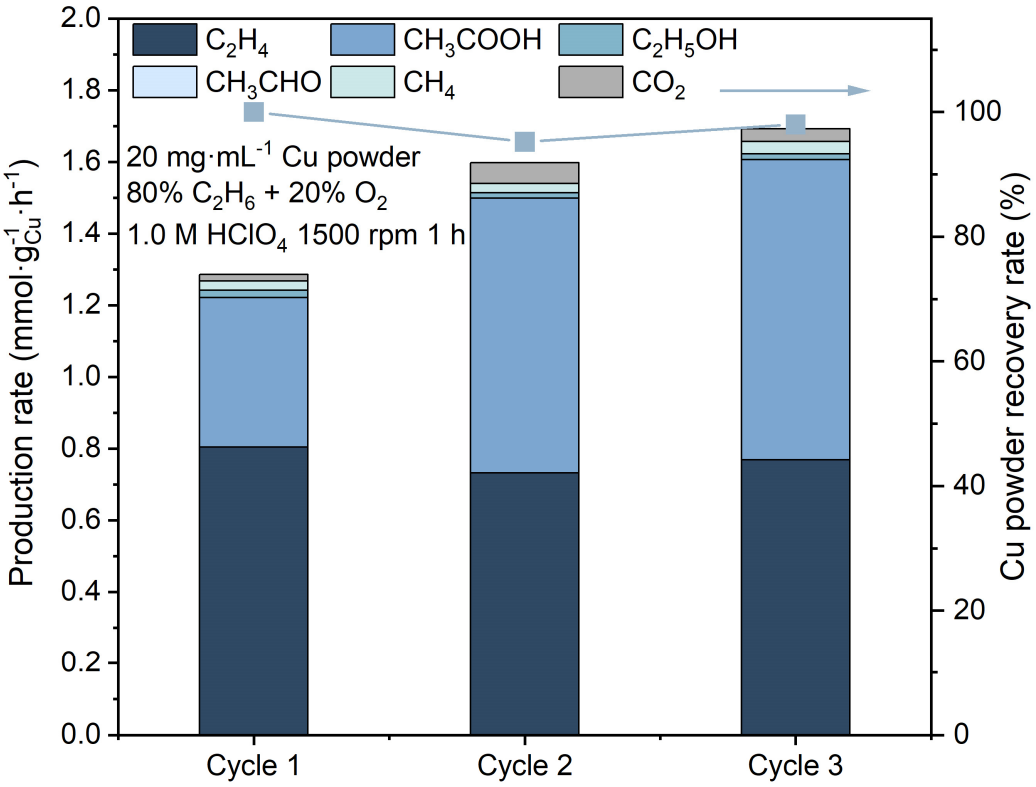

Supplementary Fig. 17 | Comparisons of ethane activation performances using recycled Cu powder and pristine commercial Cu powder in three consecutive experiments in 1.0 M $HClO_4$ at 0.2 O_2 mole fraction.

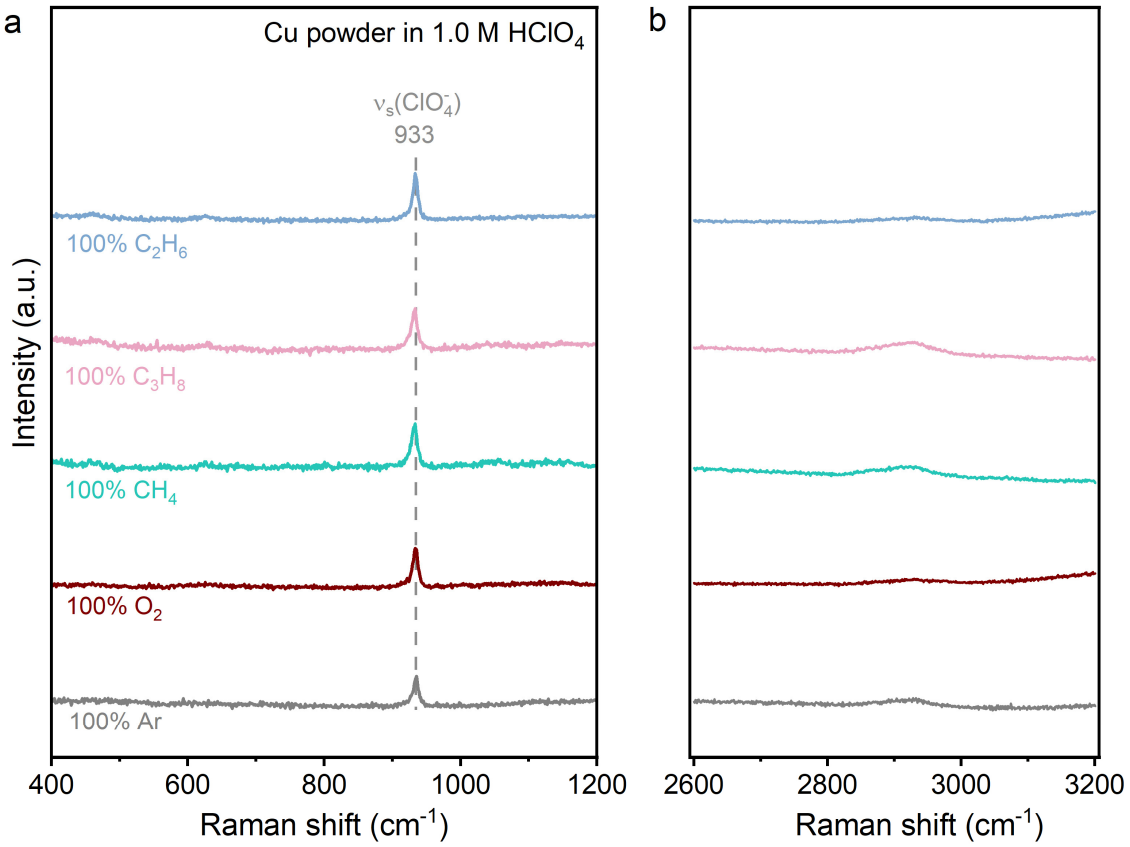

Supplementary Fig. 18 | *In situ* Raman spectra on Cu powder in 1.0 M $HClO_4$ under pure ethane, propane, methane, O_2 or Ar atmosphere.

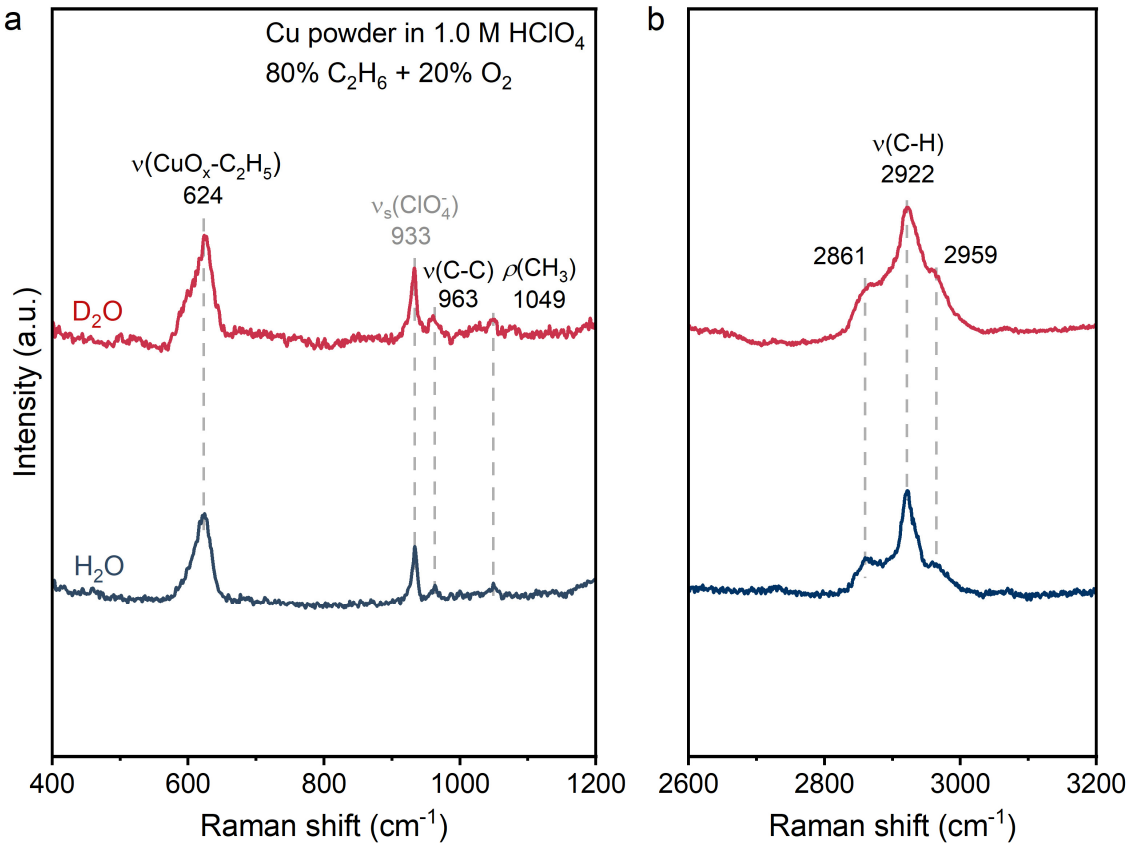

Supplementary Fig. 19 | Comparisons of *in situ* Raman spectra of ethane activation at 0.2 O_2 mole fraction using H_2O and D_2O.

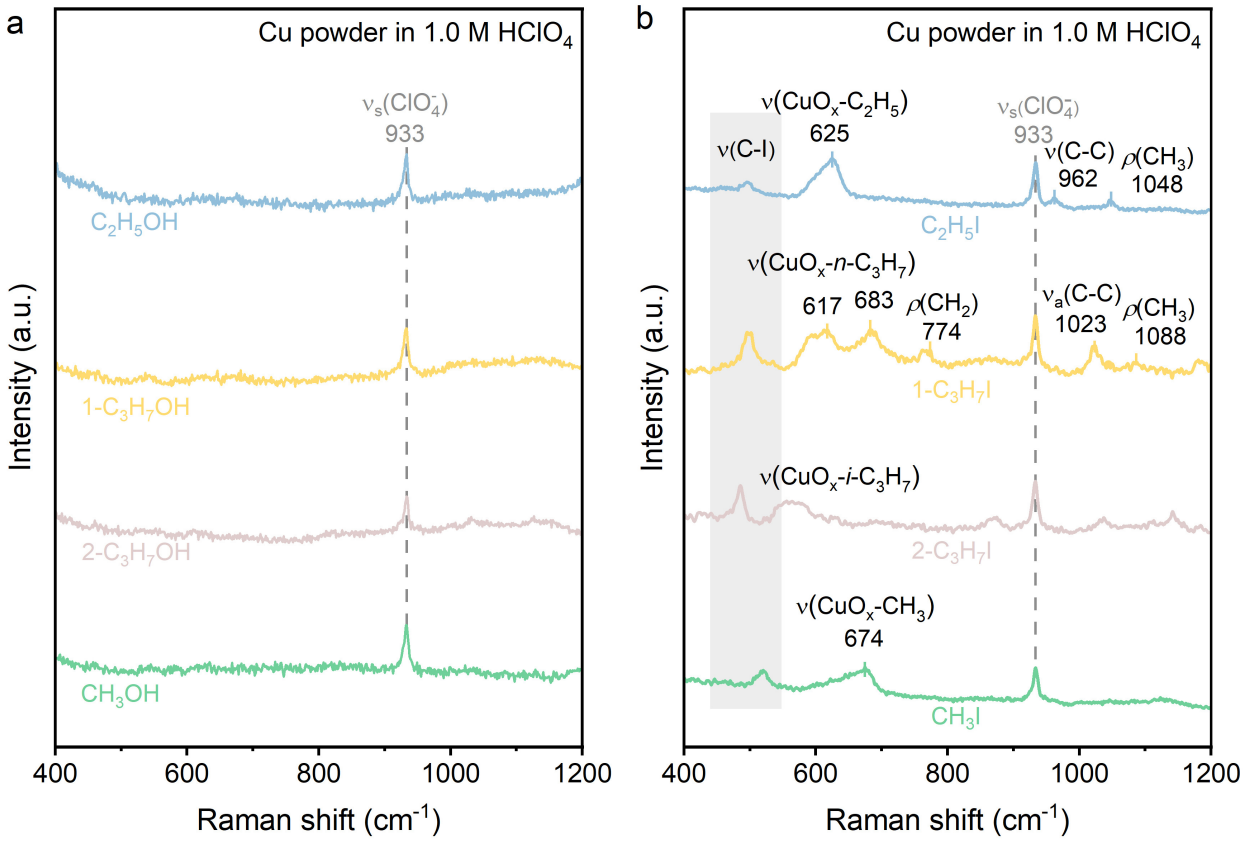

Supplementary Fig. 20 | *In situ* Raman spectra on Cu powder with a, different alcohols and b, iodoalkanes in 1.0 M $HClO_4$. Additional bands at 440~550 cm^{-1} are attributed to the stretching mode of C-I bond of undissociated iodoalkanes[1].

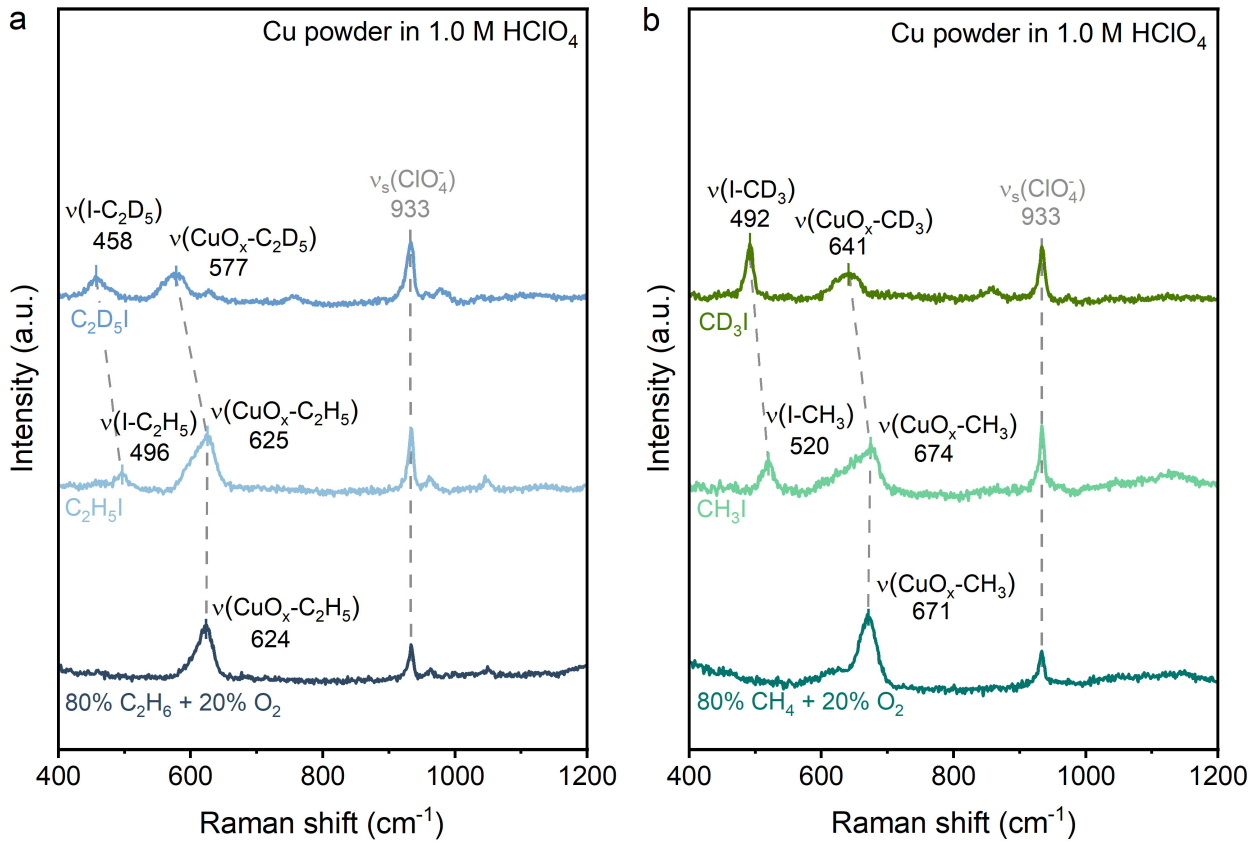

Supplementary Fig. 21 | *In situ* Raman spectra on Cu powder with **a**, deuterated iodoethane and **b**, deuterated iodomethane in 1.0 M $HClO_4$.

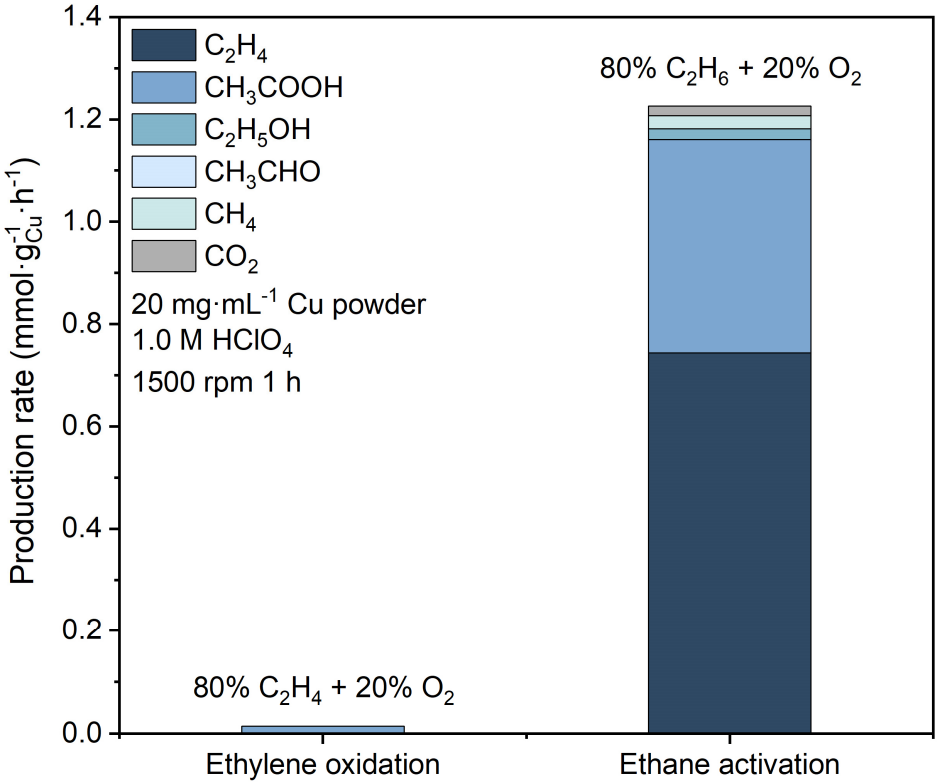

Supplementary Fig. 22 | Comparisons of production rates from ethylene oxidation and ethane activation at 0.2 O_2 mole fraction.

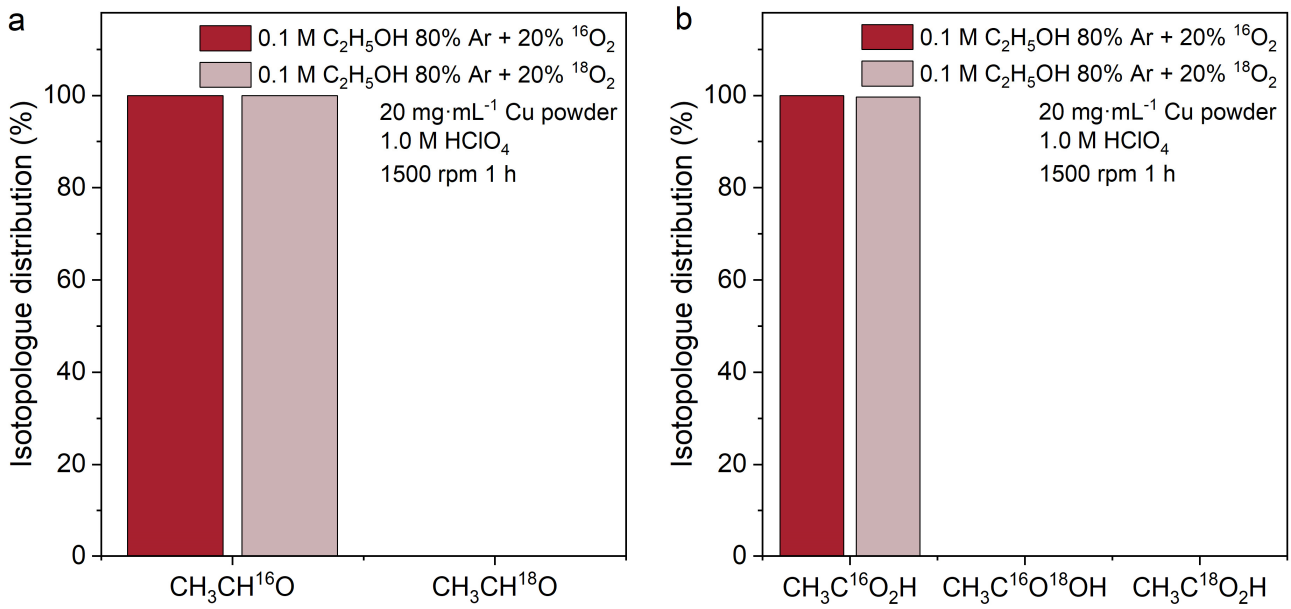

Supplementary Fig. 23 | The isotopologue distribution of ethanol oxidation products using $^{16}O_2$ or $^{18}O_2$ as gas feed.

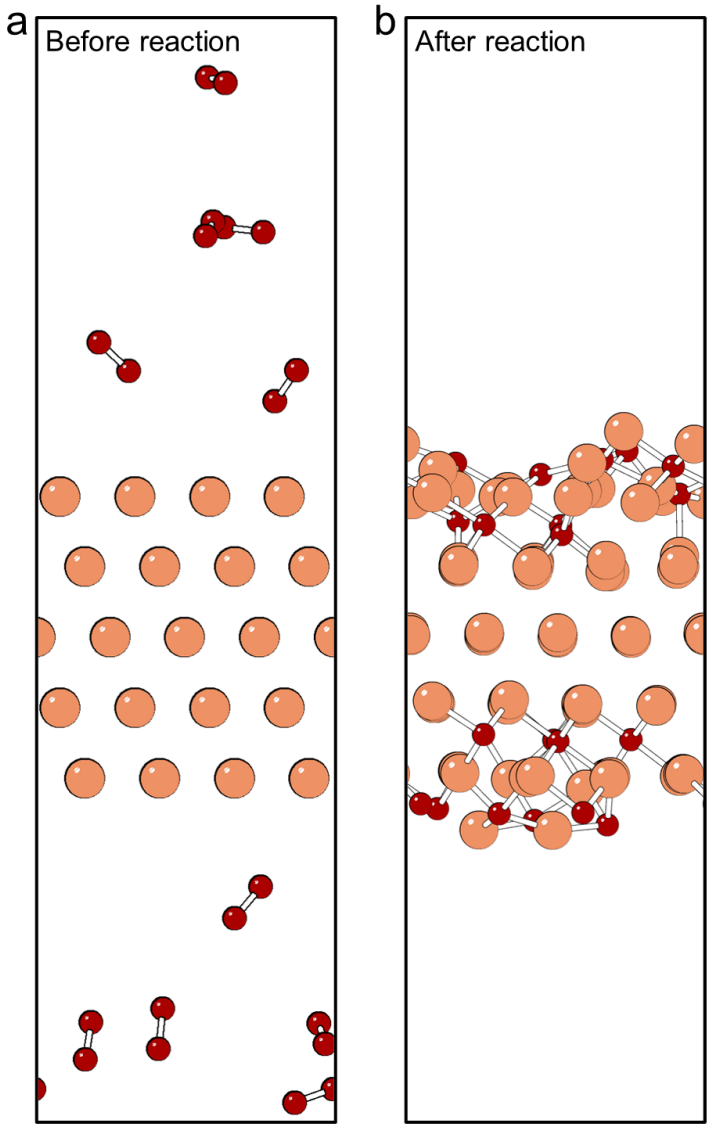

Supplementary Fig. 24 | MD simulations for the formation of Cu oxides after Cu being exposed to O_2 where orange and red spheres stand for Cu and O atoms, respectively.

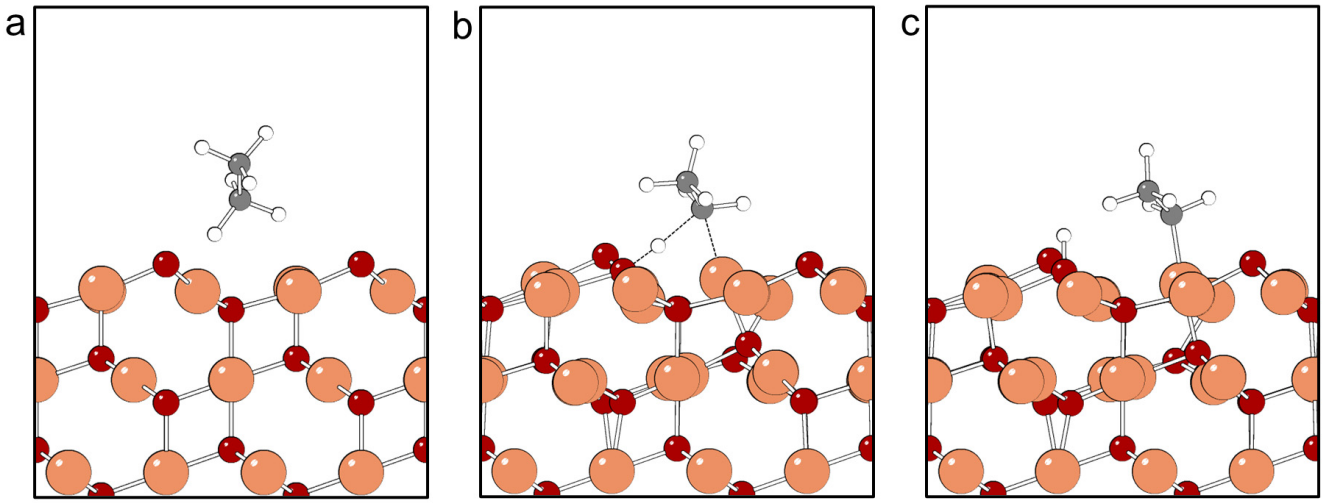

Supplementary Fig. 25 | Structures of the initial state (**a**), transition state (**b**), and final state (**c**) of the first C-H cleavage in ethane activation where orange, red, grey and white spheres stand for Cu, O, C and H atoms, respectively.

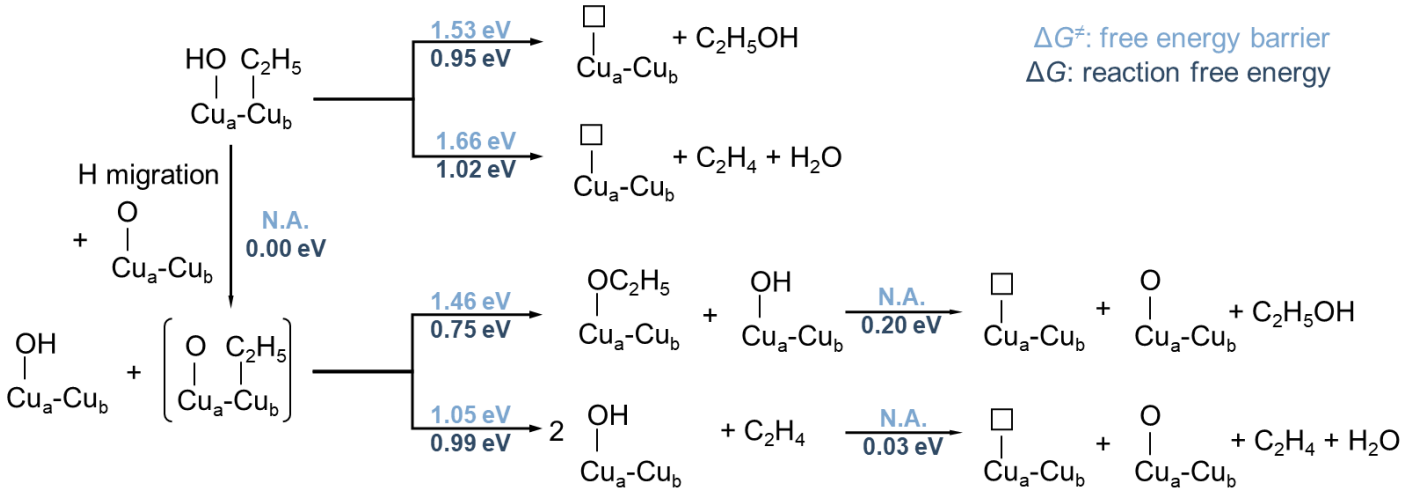

Supplementary Fig. 26 | Possible reaction pathways for ethane activation after first C-H cleavage under neutral conditions where the white square symbol stands for an oxygen vacancy and N.A. stands for no free energy barrier.

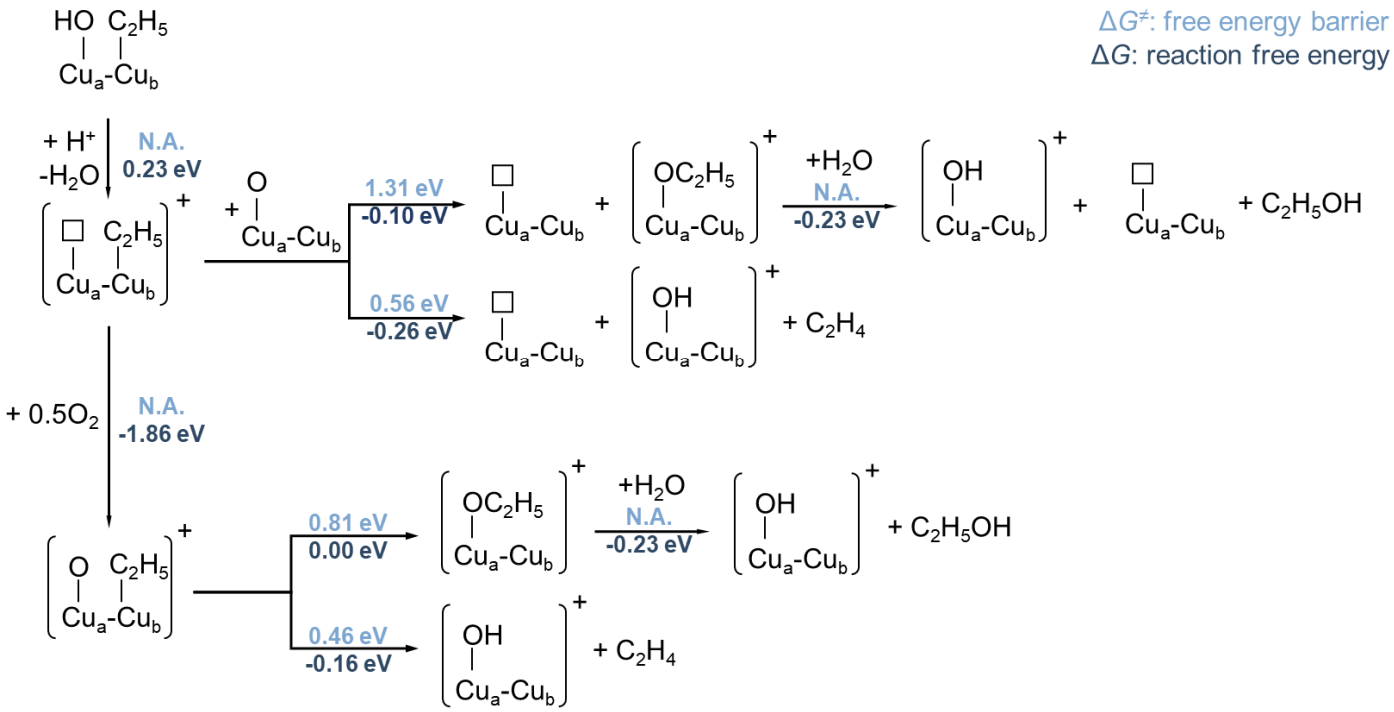

Supplementary Fig. 27 | Possible reaction pathways for ethane activation after first C-H cleavage under acidic conditions where the white square symbol stands for an oxygen vacancy and N.A. stands for no free energy barrier.

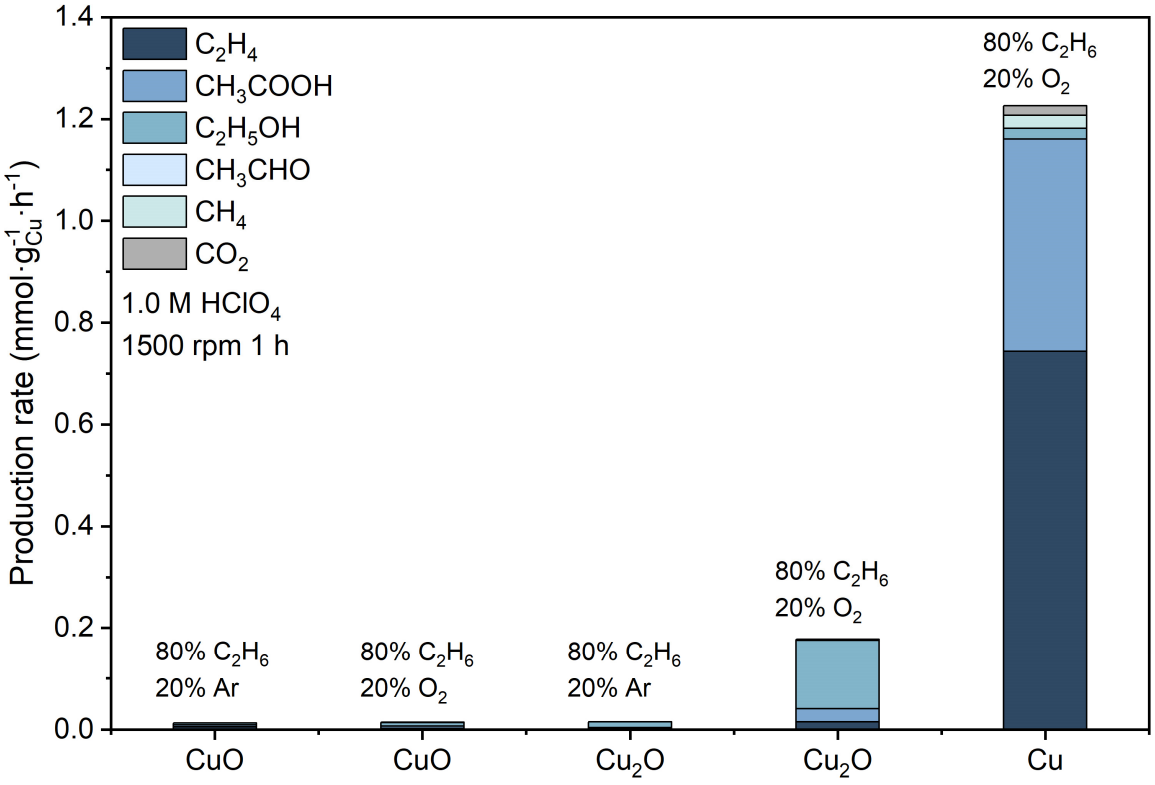

Supplementary Fig. 28 | Comparisons of ethane activation performance in 1.0 M $HClO_4$ using Cu, CuO, or Cu_2O as the catalyst.

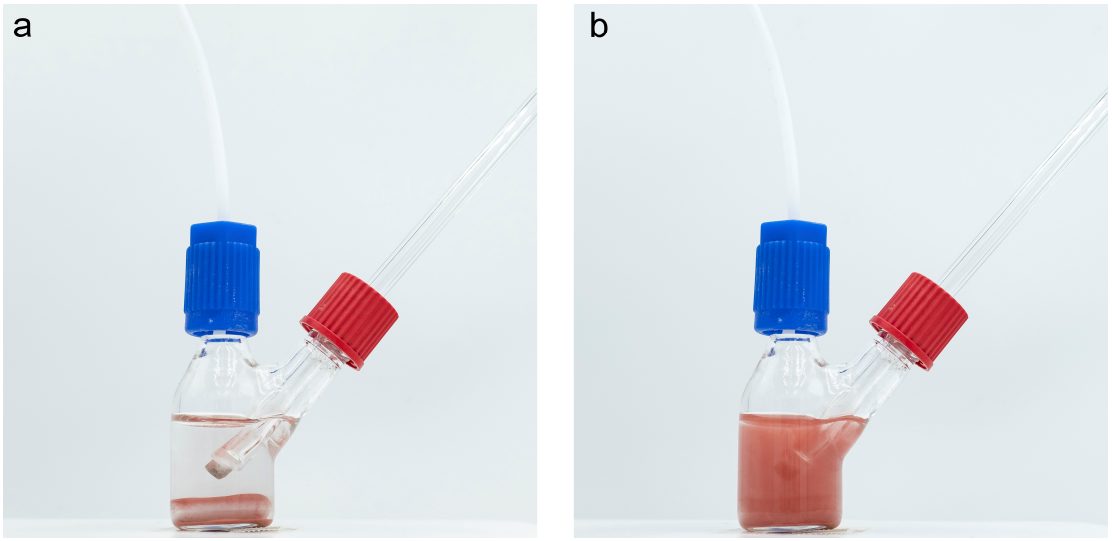

Supplementary Fig. 29 | Reaction cell employed for light alkane activation.

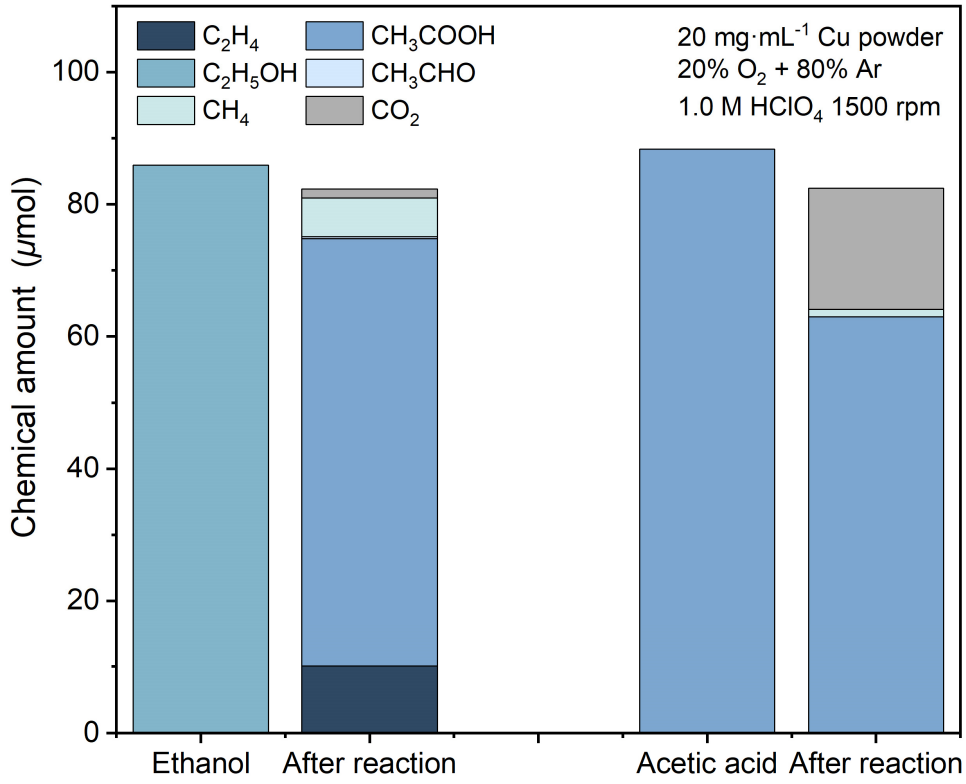

Supplementary Fig. 30 | Carbon balances for the oxidation of 10 mM ethanol and acetic acid using 20% O_2 + 80% Ar. The amount of CH_4 and CO_2 was multiplied by 0.5 because their carbon number is half of that in ethanol or acetic acid.

Supplementary Table 1 | Apparent production rates of ethane activation under various O_2 mole fractions. The unit for all production rates is $\mu mol \cdot h^{-1}$. N.D. stands for Not Detected. Data are presented as mean values ± standard deviation from four independent measurements.

O_2 mole fraction	C_2H_4	CH_3COOH	C_2H_5OH	CH_3CHO	CH_4	CO_2	C_2H_4 selectivity	CH_3COOH selectivity
0.05	63.0±4.3	32.7±2.4	5.8±0.6	N.D.	2.5±0.6	0.1±0.0	61±3.0%	32±2.3%
0.10	115.2±14.4	70.8±6.7	6.5±1.7	N.D.	4.6±0.5	1.2±0.8	59±2.6%	36±1.8%
0.20	148.8±2.7	83.4±13.0	4.2±0.4	N.D.	5.1±0.8	3.7±0.6	62±3.4%	35±3.5%
0.30	189.4±7.9	112.2±7.8	2.4±1.2	N.D.	6.5±0.4	15.9±6.1	60±1.7%	36±1.4%

Supplementary Table 2 | Apparent production rates in control experiments for ethane activation. The unit for all production rates is μmol·h^{-1}. N.D. stands for Not Detected.

Control conditions	C_2H_4	CH_3COOH	C_2H_5OH	CH_3CHO	CH_4	CO_2
No ethane, 80% Ar + 20% O_2 was used as the feed	0.01	0.3	N.D.	N.D.	N.D.	N.D.
No Cu powder	0.03	N.D.	N.D.	N.D.	N.D.	0.01
No O_2, 80% C_2H_6 + 20% Ar was used as the feed	1.8	0.1	0.35	N.D.	N.D.	0.1
0.2 M H_2O_2 was used instead of O_2, 80% ethane + 20% Ar was used as the feed	5.69	13.8	2.73	N.D.	N.D.	0.43
20 mg·mL^{-1} Pt powder was used instead of 20 mg·mL^{-1} Cu powder	0.01	0.77	N.D.	N.D.	N.D.	0.15
20 mg·mL^{-1} Pd powder was used instead of 20 mg·mL^{-1} Cu powder	0.06	0.91	N.D.	N.D.	N.D.	0.05
1.0 M $NaClO_4$ was used instead of 1.0 M $HClO_4$	0.05	N.D.	N.D.	N.D.	N.D.	0.2
0.5 M H_2SO_4 was used instead of 1.0 M $HClO_4$	166.9	69.0	3.9	N.D.	3.3	3.1
1.0 M H_3PO_4 was used instead of 1.0 M $HClO_4$	71.2	36.8	2.05	N.D.	0.22	0.5
1.0 M $C_2H_2O_4$ was used instead of 1.0 M $HClO_4$	0.24	1.41	1.24	N.D.	N.D.	23.4
0.18 M $Cu(ClO_4)_2$ + 0.64 M $HClO_4$ was used instead of 20 mg·mL^{-1} Cu powder and 1.0 M $HClO_4$	0.03	N.D.	N.D.	N.D.	N.D.	0.01
80% C_2H_4 + 20% O_2 was used as the feed	-	2.8	N.D.	N.D.	0.02	N.D.
10 mM ethanol oxidation with 80% Ar + 20% O_2	30.2	194.3	-	0.9	35.0	2.3
10 mM acetic acid oxidation with 80% Ar + 20% O_2	N.D.	-	N.D.	N.D.	6.7	108.1
25 mg·mL^{-1} CuO powder was used instead of 20 mg·mL^{-1} Cu powder, 80% ethane + 20% Ar was used as the feed	1.13	0.69	0.72	N.D.	N.D.	N.D.
25 mg·mL^{-1} CuO powder was used instead of 20 mg·mL^{-1} Cu powder, 80% ethane + 20% O_2 was used as the feed	0.51	1.33	0.94	N.D.	N.D.	0.16
22.5 mg·mL^{-1} Cu_2O powder was used instead of 20 mg·mL^{-1} Cu powder, 80% ethane + 20% Ar was used as the feed	0.61	2.25	0.17	N.D.	N.D.	0.06
22.5 mg·mL^{-1} Cu_2O powder was used instead of 20 mg·mL^{-1} Cu powder, 80% ethane + 20% O_2 was used as the feed	3.07	27	5.03	N.D.	N.D.	0.42

Supplementary Table 3 | Apparent production rates of propane activation under various O_2 mole fractions. The unit for all production rates is μmol·h^{-1}. N.D. stands for Not Detected. Data are presented as mean values ± standard deviation from four independent measurements.

O_2 mole fraction	Propylene	1-Propanol	2-Propanol	CH_3COOH	Acetone	Allyl alcohol	Propionic acid	3-Hydroxypropionic acid	CO_2	C_3H_6 selectivity
0.05	159.1±2.8	1.0±0.3	0.4±0.3	1.8±0.5	1.1±0.1	1.6±0.2	3.9±0.1	1.6±0.3	0.14±0.08	94±0.5%
0.10	216.4±13.1	1.4±0.4	0.4±0.1	1.8±0.3	2.1±0.5	3.8±0.5	5.9±0.6	4.1±0.9	0.50±0.09	92±0.4%
0.20	276.4±7.9	1.1±0.1	0.5±0.2	2.8±0.6	2.9±0.3	5.0±0.4	5.7±1.0	5.0±2.2	2.5±0.7	92±1.5%
0.30	365.4±14.5	N.D.	N.D.	8.7±2.8	7.2±1.7	12.4±2.9	12.3±1.1	11.0±1.5	6.1±1.8	88±0.4%

Supplementary Table 4 | Comparison of mass-specific C_2H_4 production rates in ethane activation between this work and previous reports.

Catalyst	Temperature (°C)	Production rates of C_2H_4 (mmol $g_{catalyst}^{-1}$ h^{-1})
This work	25	0.95
VAPO-18[2]	600	0.714
MoO_3-SiO_2-TiO_2[3]	600	1.07
NiO-Al_2O_3 + prom[4]	400	1.43
V_2O_5-TiO_2[5]	550	2.14
Ga/Cr/O-Zr/P/O[6]	400	2.14

Supplementary Table 5 | Comparison of mass-specific C_3H_6 production rates in propane activation between this work and previous reports.

Catalyst	Temperature (°C)	Production rates of C_3H_6 (mmol $g_{catalyst}^{-1}$ h^{-1})
This work	25	1.87
BS-1[7]	480	1.18
h-BN[7]	480	0.6
B_2O_3/SBA-15[8]	500	2.47
V_2O_5-SiO_2[9]	550	1.19
V-MCM-41[10]	550	0.714
MoO_3/K-SiO_2-TiO_2[11]	550	0.48
Mo/Li/O-Al_2O_3[12]	550	1.19
TS-1[13]	550	1.91

Supplementary Table 6 | Apparent production rates of methane activation under various O_2 mole fractions. The unit for all production rates is $\mu mol \cdot h^{-1}$. N.D. stands for Not Detected. Data are presented as mean values ± standard deviation from four independent measurements.

O_2 mole fraction	CO	CO_2	C_2H_6	CH_3OH	CH_3COOH	CO selectivity	CH_3OH selectivity	CH_3COOH selectivity
0.05	N.D.	10.3±0.3	N.D.	0.4±0.1	0.6±0.2	0.0±0.0%	3.7±0.9%	9.6±3.5%
0.10	0.6±0.2	19.9±2.2	0.07±0.02	0.7±0.4	0.9±0.5	2.8±0.9%	3.1±2.0%	7.7±4.3%
0.20	1.0±0.5	40.7±5.5	0.2±0.1	0.4±0.1	1.0±0.2	2.2±0.8%	0.9±0.1%	4.5±1.3%
0.30	0.8±0.3	64.1±3.4	0.05±0.01	0.6±0.3	0.5±0.1	1.2±0.4%	0.9±0.4%	1.6±0.1%

Supplementary Table 7 | Apparent production rates of ethane activation under various $HClO_4$ concentration. The unit for all productions rate is $\mu mol \cdot h^{-1}$. N.D. stands for Not Detected. Data are presented as mean values ± standard deviation from four independent measurements.

$HClO_4$ concentration	C_2H_4	CH_3COOH	C_2H_5OH	CH_3CHO	CH_4	CO_2	C_2H_4 selectivity	CH_3COOH selectivity
0.1 M	37.3±2.8	36.2±4.3	4.1±0.6	3.1±1.4	0.5±0.4	0.7±0.2	46±3.6%	45±3.0%
0.5 M	139.2±14.2	96.7±0.3	4.8±0.5	N.D.	3.9±0.6	4.1±1.7	57±2.5%	40±2.3%
1.0 M	148.8±2.7	83.4±13.0	4.2±0.4	N.D.	5.1±0.8	3.7±0.6	62±3.4%	35±3.5%
2.0 M	162.0±6.7	69.8±4.8	2.6±1.5	N.D.	10.2±1.0	4.8±0.4	67±1.4%	29±1.5%

Supplementary Table 8 | Apparent production rates of ethane activation under various loadings of Cu powder. The unit for all production rates is $\mu mol \cdot h^{-1}$. N.D. stands for Not Detected. Data are presented as mean values ± standard deviation from four independent measurements.

Cu powder loading	C_2H_4	CH_3COOH	C_2H_5OH	CH_3CHO	CH_4	CO_2	C_2H_4 selectivity	CH_3COOH selectivity
5 $mg \cdot mL^{-1}$	58.5±7.4	50.8±4.7	3.6±0.5	N.D.	2.0±0.6	8.4±1.8	50±2.3%	43±1.8%
10 $mg \cdot mL^{-1}$	146.1±7.0	81.4±5.0	4.1±0.1	N.D.	6.1±1.4	9.50±1.92	61±1.4%	34±0.9%
20 $mg \cdot mL^{-1}$	148.8±2.7	83.4±13.0	4.2±0.4	N.D.	5.1±0.8	3.7±0.6	62±3.4%	35±3.5%
40 $mg \cdot mL^{-1}$	152.5±7.8	78.6±3.6	2.0±1.7	N.D.	5.6±0.5	4.2±0.8	64±2.0%	33±2.1%

Supplementary Table 9 | Apparent production rates of ethane activation under various stirring rates. The unit for all production rates is μmol·h^{-1}. N.D. stands for Not Detected. Data are presented as mean values ± standard deviation from four independent measurements.

Stirring rate	C_2H_4	CH_3COOH	C_2H_5OH	CH_3CHO	CH_4	CO_2	C_2H_4 selectivity	CH_3COOH selectivity
400 rpm	42.5±1.0	26.0±8.7	5.9±0.7	N.D.	1.6±0.8	0.8±0.4	56±5.8%	34±7.2%
625 rpm	62.2±1.8	34.9±10.2	5.8±0.7	0.1±0.2	2.0±0.4	2.3±1.5	59±5.4%	33±6.1%
900 rpm	117.1±4.2	75.6±9.6	4.9±0.6	0.5±0.1	4.2±1.2	4.2±0.4	58±3.6%	37±3.9%
1225 rpm	140.2±16.9	86.1±11.0	3.6±2.8	0.7±0.2	4.8±0.5	4.3±0.7	60±0.6%	37±0.9%
1500 rpm	148.8±2.7	83.4±13.0	4.2±0.4	N.D.	5.1±0.8	3.7±0.6	62±3.4%	35±3.5%

Supplementary Table 10 | Mass of the dissolved Cu powder after reaction for 1 h at different gas feeds with 20 mg·mL^{-1} Cu loading at 1500 rpm. The initial mass of Cu powder is 200 mg and the volume of the solution is 10 mL. Data are presented as mean values ± standard deviation from four independent measurements.

Gas feed	Mass of remaining Cu (mg)	Cu dissolution rate (μmol·h^{-1})	Cu^{2+} concentration (M)
Propane (80%) + O_2 (20%)	88±8	1762±126	0.176±0.012
Ethane (80%) + O_2 (20%)	85±7	1804±110	0.180±0.012
Methane (80%) + O_2 (20%)	77±13	1941±205	0.194±0.021
Ar (80%) + O_2 (20%)	70±1	2049±16	0.205±0.001

Supplementary Table 11 | ^{1}HNMR information for commercial authentic standards in H_2O/D_2O with a molar ratio of 5:1.

Chemical shift (ppm)	Formular	Species	^{1}H splitting
0.050	CH_4	Methane	s
0.692	C_2H_6	Ethane	s
0.745	$CH_3CH_2CH_3$	Propane	t
0.763	$CH_3CH_2CH_2OH$	1-Propanol	t
0.775	$CH_3CH_2CH_2CH_2OH$	1-Butanol	t
0.872	$CH_3COCH_2CH_3$	Butanone	t
0.923	CH_3CH_2CHO	Propionaldehyde	t
0.962	CH_3CH_2COOH	Propionic acid	t
1.044	$CH_3CHOHCH_3$	2-Propanol	d
1.054	CH_3CH_2OH	Ethanol	t
1.123	$CH_3COOCH_2CH_3$	Ethyl acetate	t
1.160	$CH_3CH_2CH_3$	Propane	septet
1.204	$CH_3CH(OH)_2$	Acetaldehyde hydrate	d
1.218	$CH_3CH_2CH_2CH_2OH$	1-Butanol	sextet
1.400	$CH_3CH_2CH_2CH_2OH$	1-Butanol	quintet
1.418	$CH_3CH_2CH_2OH$	1-Propanol	sextet
1.955	$CH_3COOCH_2CH_3$	Ethyl acetate	s
1.962	CH_3COOCH_3	Methyl acetate	s
1.966	CH_3COOH	Acetic acid	s
2.024	$HOCH_2COCH_3$	Hydroxyacetone	s
2.075	$CH_3COCH_2CH_3$	Butanone	s
2.100	CH_3COCH_3	Acetone	s
2.116	CH_3CHO	Acetaldehyde	d
2.274	CH_3CH_2COOH	Propionic acid	q
2.437	CH_3CH_2CHO	Propionaldehyde	octet
2.455	$CH_3COCH_2CH_3$	Butanone	q
2.491	$HOOCCH_2CH_2OH$	3-Hydroxypropionic acid	t
2.600	CH_3SOCH_3	DMSO	s
3.232	CH_3OH	Methanol	s
3.435	$CH_3CH_2CH_2OH$	1-Propanol	t
3.484	$CH_3CH_2CH_2CH_2OH$	1-Butanol	t
3.531	CH_3CH_2OH	Ethanol	q
3.543	$HOCH_2CH_2OH$	Ethylene glycol	s
3.554	CH_3COOCH_3	Methyl acetate	s
3.732	$HOOCCH_2CH_2OH$	3-Hydroxypropionic acid	t
3.895	$CH_3CHOHCH_3$	2-Propanol	septet
3.985	CH_2CHCH_2OH	Allyl alcohol	qt
4.015	$CH_3COOCH_2CH_3$	Ethyl acetate	q
4.245	$HOCH_2COCH_3$	Hydroxyacetone	s
5.06	CH_2CHCH_2OH	Allyl alcohol	d
5.115	$CH_3CH(OH)_2$	Acetaldehyde hydrate	q
5.16	CH_2CHCH_2OH	Allyl alcohol	d
5.884	CH_2CHCH_2OH	Allyl alcohol	t
6.796	C_6H_5OH	Phenol	d
6.866	C_6H_5OH	Phenol	t
7.200	C_6H_5OH	Phenol	t
8.111	$HCOOH$	Formic acid	s
9.537	CH_3CHO	Acetaldehyde	s
9.569	CH_3CH_2CHO	Propionaldehyde	t

Supplementary References

1. Phillips, D. L., Lawrence, B. A. & Valentini, J. J. Substituent effects on gas-phase photodissociation dynamics: resonance Raman spectra of ethyl iodide, isopropyl iodide, and tert-butyl iodide. *J. Phys. Chem.* **95**, 9085-9091 (1991).

2. Concepción, P., Blasco, T., López Nieto, J. M., Vidal-Moya, A., Martínez-Arias, A. Preparation, characterization and reactivity of V- and/or Co-containing AlPO-18 materials (VCoAPO-18) in the oxidative dehydrogenation of ethane. *Micropor. Mesopor. Mater.* **67,** 215-227 (2004).

3. Watson, R. B., Ozkan, U. S. Mo Loading Effects over Mo/Si : Ti Catalysts in the Oxidative Dehydrogenation of Ethane. *J. Catal.* **208**, 124-138 (2002).

4. Heracleous, E., Lee, A., Wilson, K., Lemonidou, A. Investigation of Ni-based alumina-supported catalysts for the oxidative dehydrogenation of ethane to ethylene: structural characterization and reactivity studies. *J. Catal.* **231,** 159-171 (2005).

5. Heracleous, E., Machli, M., Lemonidou, A. A., Vasalos, I. A. Oxidative dehydrogenation of ethane and propane over vanadia and molybdena supported catalysts. *J. Mol. Catal. A Chem.* **232,** 29-39 (2005).

6. Solsona, B., López-Nieto, J. M., Alcántara-Rodríguez, M., Rodríguez-Castellón, E., Jiménez-López, A. Oxidative dehydrogenation of ethane on Cr, mixed Al/Cr and mixed Ga/Cr oxide pillared zirconium phosphate materials. *J. Mol. Catal.A Chem.* **153,** 199-207 (2000).

7. Zhou, H., Yi, X., Hui, Y., Wang, L., Chen, W., Qin, Y., Wang, M., Ma, J., Chu, X., Wang, Y., Hong, X., Chen, Z., Meng, X., Wang, H., Zhu, Q., Song, L., Zheng, A., Xiao, F. S. Isolated boron in zeolite for oxidative dehydrogenation of propane. *Science* **372,** 76-80 (2021).

8. Lu, W. D., Wang, D., Zhao, Z., Song, W., Li, W.-C., Lu, A. H. Supported Boron Oxide Catalysts for Selective and Low-Temperature Oxidative Dehydrogenation of Propane. *ACS Catal.* **9,** 8263-8270 (2019).

9. Liu, Y., Feng, W., Li, T., He, H., Dai, W., Huang, W., Cao, Y., Fan, K. Structure and catalytic properties of vanadium oxide supported on mesocellulous silica foams (MCF) for the oxidative dehydrogenation of propane to propylene. *J. Catal.* **239,** 125-136 (2006).

10. Peña, M. L., Dejoz, A., Fornés, V., Rey, F., Vázquez, M. I., López Nieto, J. M. V-containing MCM-41 and MCM-48 catalysts for the selective oxidation of propane in gas phase. *Appl. Catal. A: Gen.* **209,** 155-164 (2001).

11. Watson, R. B., Ozkan, U. S. K/Mo Catalysts Supported over Sol-Gel Silica-Titania Mixed Oxides in the Oxidative Dehydrogenation of Propane. *J. Catal.* **191,** 12-29 (2000).

12. Abello, M. Characterization and performance for propane oxidative dehydrogenation of Li-modified MoO_3/Al_2O_3 catalysts. *Appl. Catal. A: Gen.* **251,** 435-447 (2003).

13. Schuster, W., Niederer, J. P. M., Hoelderich, W. F. The gas phase oxidative dehydrogenation of propane over TS-1. *Appl. Catal. A: Gen.* **209,** 131-143 (2001).